9th IAA Planetary Defense Conference – PDC 2025
5-9 May 2025, Stellenbosch, Cape Town, South Africa

IAA-PDC-25-06-52

HYPERVELOCITY CRATERING AND DISRUPTION OF THREE L-TYPE ORDINARY CHONDRITES: EFFECTS OF STRENGTH AND POROSITY ON DISRUPTION ENERGY

George J. Flynn[1], Melissa Strait[2], Daniel D. Durda[3], and Robert Macke[4]
[1]*SUNY-Plattsburgh, 101 Broad St., Plattsburgh NY 12901 USA (george.flynn@plattsburgh.edu),*
[2]*Alma College, Alma, MI 48801 (straitm@alma.edu),*
[3]*Southwest Research Institute, 1301 Walnut Street, Suite 400, Boulder CO 80302 (durda@boulder.swri.edu),*
[4]*Vatican Observatory, V-00120 Vatican City(macke@jesuits.net)*

Abstract

The response of asteroids to hypervelocity impact influences momentum transfer in cratering and fragmentation in disruptive collisions, which together limit the maximum change in velocity (ΔV_{MAX}) that can be imparted by a single kinetic impact. For Q_F, the energy per unit target mass for onset of fragmentation, β, the ratio of impactor momentum to momentum acquired by the target, and v_i, the impactor mass: $\Delta V_{MAX} = 2Q_F\beta/v_i$. Hydrocode modeling indicates β decreases with increasing target porosity, and, Q^*_C, the energy for the onset of catastrophic disruption, increases with increasing target porosity or decreasing target strength. To test this, we performed hypervelocity cratering and disruption experiments on three asteroid samples of similar compositions but different porosities (P) and compressive strengths (S): the low porosity L3 Ordinary Chondrite (OC) meteorite Aba Panu (P ~3.1%, S = 438 MPa), the intermediate porosity L3-6 OC Northwest Africa 869 (NWA 869) (P ~7.8%, S = 87 MPa), and the high porosity L4 OC Saratov (P ~14.1%, S = 0.97 MPa). β followed the pattern expected from modeling: β = 3.5 for Aba Panu, 2.7 for NWA 869, and 2.5 for Saratov. However, the decrease in β with increasing porosity is not as strong as suggested by hydrocode modeling. The energy required for catastrophic disruption (Q^*_C) deviated from modeling that indicates more porous targets should be more resistant to disruption. Saratov gave Q^*_C = 1,090 J/kg, comparable to the low-porosity OC Aba Panu (Q^*_C = 1,230 J/kg) but much lower than the 1,990 J/kg we measured for the intermediate porosity OC NWA 869. Earlier work by other investigators proposed that for disruptive events Q^*_C is proportional $S^{0.45}$. Using this approach, we found a power law behavior between $Q^*_C/S^{0.45}$ and (1 – P), indicating that, for these three L-type OCs, the dependence of Q^*_C on strength can be separated from the dependence on porosity. Further, we determined Q^*_F, the energy per unit target mass for the onset of fragmentation, and calculated ΔV_{MAX}, for each ordinary chondrite There is only a small difference between ΔV_{MAX} values for these three meteorites vary, which vary from 0.61 to 1.32 m/s, compared to the factor-of-seven difference we reported between NWA 869 and the anhydrous carbonaceous chondrite Northwest Africa 4502. This suggests remote sensing demonstrating an asteroid is similar to an L-type OC may be sufficient for selecting the impactor mass and speed for a kinetic impact deflection that avoids significant fragmentation.

Keywords: Hypervelocity Impact Cratering, Hypervelocity Impact Fragmentation, Meteorites, Ordinary Chondrites, Kinetic Impact Deflection

1. Introduction

Kinetic impact deflection, which was demonstrated by the NASA Double Asteroid Redirection Test (DART) spacecraft [1], is regarded as the most mature technology currently available for deflection of a monolithic asteroid up to a few hundred meters in diameter that is on a collision course with the Earth [2]. However, a successful kinetic impact deflection requires a knowledge of the momentum added by the impact or sequence of impacts as well as the maximum kinetic energy that can be deposited in the target without fragmentation, since this could leave a fragment of the target on a collision course with the Earth.

The momentum transferred to a monolithic rock target in a hypervelocity kinetic impact is observed to be greater than the original momentum of the projectile because of the ejection of cratering debris in a direction approximately opposite to the flight direction of the projectile. In a cratering impact on a monolithic target the recoil momentum has contributions from two factors:

1) the momentum of the impactor, and,
2) the momentum provided by the crater ejecta.

The total momentum transferred in a cratering impact is characterized by a factor β, which is the ratio of the increase in momentum of the target to the momentum of the projectile, where:

$$\beta = 1 + p_e/p_i \qquad \text{(Equation 1)}$$

where p_e is the momentum of the crater ejecta and p_i is the impactor momentum. So, β is 1 in the absence of crater ejecta and (β -1) is the momentum enhancement from the crater ejecta.

To avoid fragmentation, which could leave a large piece of the target asteroid on a collision course with Earth, the maximum change in velocity, ΔV_{max}, that can be achieved in a single kinetic impact is restricted by the requirement:

$$\Delta V_{max} = 2\ \beta\ Q^*_F/v_i \qquad \text{(Equation 2)}$$

where Q^*_F is the energy per unit target mass where the outcome of an impact transitions from cratering to fragmentation, and v_i is the speed of the impactor relative to the asteroid [3]. Thus, both β and Q^*_F must be known for the asteroid in question in order to design a successful kinetic impact deflection mission.

Modeling of hypervelocity impacts has provided insights into the expected dependance of collisional outcomes, particularly β and Q^*_F, on the strength and porosity of the target asteroid. Compaction of porous material is expected to help absorb the impact energy and reduce the transmission of shock, localizing much of the damage to the immediate region of the impact [4]. The impact modeling generally indicates that lower strength and/or higher porosity increases the collisional survival of a monolithic asteroid by requiring a higher energy for fragmentation [5, 6]. However, most of this modeling employs the physical properties of terrestrial rocks.

Asteroids span a wide diversity of mineralogical compositions, porosities, and strengths. Stickle et al. [5, 6] showed that the two most important physical properties

of the target affecting the modeled outcome of hypervelocity impact are the target strength and the target porosity. Thus, a knowledge of the strength, porosity, and likely the mineralogical composition of the target asteroid are each critical in insuring a successful kinetic impact deflection. The mineralogical composition of an asteroid can be determined remotely by reflection spectroscopy using terrestrial or space-based telescopes. However, the porosity of an asteroid is usually determined by gravitational perturbation. This requires either another relatively nearby, large asteroid or a flyby spacecraft. A strength determination generally requires a lander spacecraft to sample and test the underlying bedrock.

Meteorites provide laboratory samples of their asteroidal parent bodies, allowing measurement of the porosity and strength of samples of a variety of asteroid parent bodies. The recovered meteorites provide direct evidence for the diversity of mineralogies, strengths, and porosities among the Near-Earth Objects (NEOs). However, the weakest meteors fragment so severely during atmospheric deceleration that this group is not well sampled by the meteorites since only dust survives.

The recovered meteorites range from the weak, highly porous CI1 carbonaceous chondrites like Orgueil to the strong, low porosity iron meteorites like Canyon Diablo. The types and relative frequencies of meteorite falls provide some indication of the mineralogy, porosity, and strength range of the population of NEOs. The recovery of observed meteorite falls provides an indication of the relative abundance of each type in near-Earth space. Iron meteorites constitute less than 4% of all falls, stony-iron meteorites about 1.0%, and stony meteorites about 95%.

The ordinary chondrites are the most common stony meteorites that fall to Earth. Among the ordinary chondrites, there are three distinct types based on their mineralogies: the high-iron or H-type, the low-iron or L-type, and the very low iron or LL-type. The physical properties, including the mineralogies, the porosities, and the compressional and tensile strengths, of the stone meteorites, which constitute about 95% of all meteorite falls, were summarized in reviews by Flynn et al. [7] and Ostrowski and Bryson [8]. These reviews are consistent with the observation of Slyuta et al. [9] that: “There are no analogues among terrestrial igneous and sedimentary rocks and ores… [for the] set of physical and mechanical properties of the meteorites.” Slyuta et al. [9] indicated that knowledge of meteorite or meteorite-analog physical properties is critical to estimating the hazard of asteroidal impacts, creating engineering models for asteroid sample collection, and understanding the requirements for asteroid deflection.

2. Samples

To characterize the response of asteroid material to hypervelocity impacts we performed hypervelocity impact cratering and disruption experiments on three L-type ordinary chondrite meteorites, Aba Panu, Northwest Africa 869 (NWA 869), and Saratov. Since all three a L-type ordinary chondrites, they have very similar mineralogies, and thus similar remote sensing spectra. These three L-type meteorites were selected for our study because they were minimally weathered by exposure on the Earth, they were not severely shocked during residence near the surface and during ejection from their parent bodies, and they were available in sufficient quantity and size for the experiments. These three L-type ordinary chondrites span most of the strength range and much of the porosity range of the ordinary chondrite meteorites.

Table 1: Physical Properties and Impact Outcomes for three L-type Meteorites.

Meteorite	Type	Porosity (%)	Comp. Strength (MPa)	Speed of Sound (m/s)	β	Q^*_C J/kg)	Q^*_F (J/kg)	ΔV_{max} at ~5 km/s
Aba Panu	L3	3.1	438	5,100	3.7	1,230	680	1.01
NWA 869	L3-6	7.8	87	3,280	2.5	1,990	1320	1.32
Saratov	L4	14.1	0.97	2,350	2.3	1,090	660	0.61

We performed physical properties measurements, including the bulk and grain densities, allowing determination of the porosity, the unconfined compressive strength, the speed of sound, and Young's modulus on each of the three meteorites (Table 1). The grain volume was determined using Ideal Gas Pycnometry and the bulk volume was determined by laser scanning to target, as described by Macke et al. [10, 11]. These values were used to determine the grain density (ρ_g) and the bulk density (ρ_b) of each target type. The target porosity (P) was then determined using:

$$P = 1 - \rho_b/\rho_g \qquad \text{(Equation 3)}$$

The unconfined compressive strengths of NWA 869 and of Saratov were measured on 1 cm cubes of each meteorite by applying a pressure across two opposite faces of each cube using a hydraulic press to slowly increase the pressure until failure occurred. The strength of Aba Panu is from Cotto-Figueroa et al. [12] The speed of sound of Aba Panu and NWA 869 were measured using an ultrasonic thickness gauge in a mode that determines the sound speed when the sample thickness is known [13]. The speed of sound of Saratov samples was determined in earlier work [14].

These three L-type ordinary chondrites selected for our measurements span most of the range of porosity, and strength of the ordinary chondrite meteorites.

Aba Panu is a low porosity L3 ordinary chondrite. It is a fresh fall, having a low degree of terrestrial weathering (W0), but is somewhat shocked (S4).

NWA 869 is an intermediate porosity, brecciated L3-6 ordinary chondrite. NWA 869 is a find, but it experienced a low degree of terrestrial weathering (W1) and lesser shock (S3) than Aba Panu.

Saratov is a high porosity L4 ordinary chondrite. It is an observed fall having a low degree of terrestrial weathering (W0), but is somewhat shocked (S4).

2. Hypervelocity Impact Experiments

We conducted hypervelocity impact cratering and disruption measurements at the NASA Ames Vertical Gun Range (AVGR). Each target was suspended from the ceiling of the sample chamber on an ~2 m long fishing line. This allowed the targets to recoil freely in cratering experiments and did not interfere with the disruption in fragmentation experiments. The sample chamber was pumped to ~0.5 torr to minimize atmospheric interference with the projectile. The impactors were solid aluminum spheres having diameters of 1/16", 1/8", or 1/4" aimed at the center of each target. The speed of each impactor was determined using a laser-interrupt system. The impactor speeds ranged from 4.0 to 5.8 km/s. The AVGR and its gun chamber are described in detail by Karz et al. [15]. Some of the hypervelocity cratering and disruption results for the NWA 869

meteorite were described in an earlier paper [16], which includes a complete description of the experimental setup employed for these measurements.

For the fragmentation impacts all of the target material was recovered from the gun chamber after each impact. The mass of the largest fragment produced in the impact, M_L, was compared to the initial mass of the target, M_T. Since no two individual rocks, even from the same material, are identical in flaw distribution, shape, etc., the energy required for fragmentation is usually determined from the outcomes of a series of impacts conducted at different impactor specific energies, Q*, the impactor kinetic energy per unit target mass [17]. The energy for the onset of catastrophic disruption Q^*_C, is determined from a plot of M_L/M_T vs. Q* [17]. Q^*_C is generally regarded as the impactor energy where the mass of the largest fragment produced in the impact is one-half the target mass. Q^*_C is the value of Q* where a horizontal line at $M_L/M_T = 0.5$ intersects the best fit line to the fragmentation data (Figure 1). To determine Q^*_F, the energy for the onset of fragmentation, we extended the best fit line for M_L/M_T vs Q* to the point where it intersected $M_L/M_T = 0.98$, which corresponds to a cratering impact.

Figure 1: M_L/M_T vs Q* for Aba Panu.

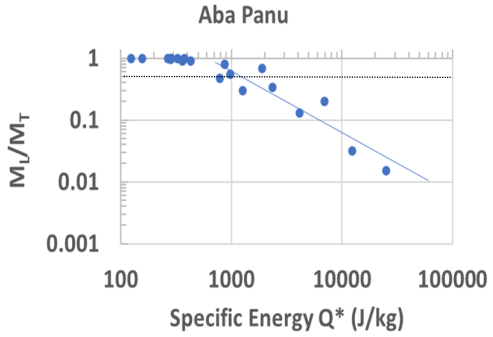

Figure 2: M_L/M_T vs Q* for NWA 869.

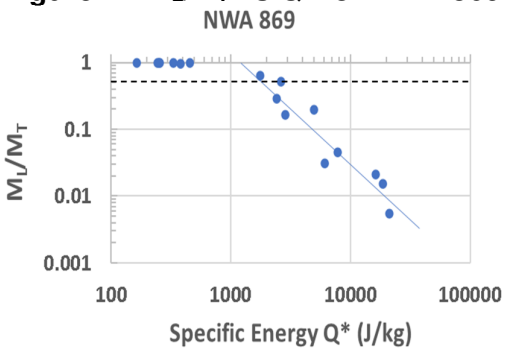

Figure 3: M_L/M_T vs Q* for Saratov.

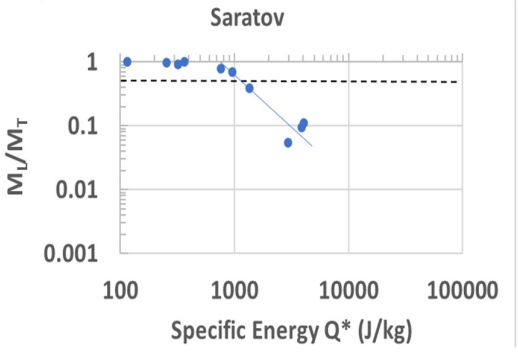

We performed ten fragmentation impacts on Aba Panu at specific energies ranging from 791 J/kg to 24,901 J/kg. These impacts gave M_L/M_T values ranging from 0.015 to 0.806 (Figure 1). The best fit line to this data set gives Q^*_C =1,230 J/kg and Q^*_F = 680 J/kg. The ten fragmentation impacts on NWA 869 were conducted at energies ranging from 1,764 J/kg to 21,225 J/kg resulting in M_L/M_T values ranging from 0.016 to 0.639 (Figure 2). The best fit line to these impacts gives Q^*_C =1,990 J/kg and Q^*_F = 1,320 J/kg. Seven fragmentation impacts were performed on Saratov at specific energies ranging from 708 J/kg to 4,069 J/kg resulting in M_L/M_T values ranging from 0.055 to 0.889 (Figure 3). The best fit line to these impacts gives Q^*_C =1,090 J/kg and Q^*_F = 660 J/kg.

For each cratering experiment marked grids were placed below and behind each target. A high-speed video camera was placed above the target and second high-speed video camera was placed in front of the target to record each impact. The resulting target recoil speed was determined from the target motion relative to the grids in a sequence of frames taken after each impact. From this recoil speed, the target

mass, and the impactor mass and speed we determined the value of β. We also determined the mass of the crater ejecta (M_T - M_L), measured the depth and the diameter of the crater, and determined the shape of the crater. The speeds of some of the larger ejecta fragments were also determined to ensure consistency between the measured recoil speed and the momentum carried by the crater ejecta. On the plots of M_L/M_T vs Q* these cratering impacts scatter around a horizontal line near M_L/M_T = 0.98 (Figures 1, 2, and 3)).

We performed ten cratering experiments on Aba Panu at specific energies ranging from 124 J/kg to 430 J/kg (Figure 1). These impacts gave a value of β = 3.7. The mass of the crater ejecta ranged from 1 g to 5 g. with a mean of 2.8 g. We performed seven cratering experiments on NWA 869 at specific energies ranging from 165 J/kg to 460 J/kg (Figure 2). These impacts gave a value of β = 2.5. The mass of the crater ejecta ranged from <0.5 g to 5 g. with a mean of 2.6 g. We performed four cratering experiments on NWA 869 at specific energies ranging from 115 J/kg to 363 J/kg (Figure 3). These impacts gave a value of β = 2.3. The mass of the crater ejecta ranged from 2 g to 3 g. with a mean of 2.3 g. The craters in Aba Panu and NWA 869 were approximately bowl shaped with depths approximately one-half their diameters. The craters in Saratov were more elongated, approximating a cylindrical shape.

3. Discussion

Saratov has the lowest compressive strength and the highest porosity of any of these three, L-type ordinary chondrites we measured. Based on hydrocode modeling, Saratov was expected to be the most resistant of the three L-type ordinary chondrites to fragmentation or disruption (i.e., have highest Q^*_F and Q^*_C). However, Saratov had the lowest Q^*_F and Q^*_C of these three meteorites.

The ordinary chondrite meteorites have a two-component structure: strong, low porosity chondrules consisting of crystalline olivine or pyroxene, embedded in a weaker, more porous matrix. The increase in porosity generally corresponds to an increase in the matrix porosity, leaving larger pore spaces that result in a decrease in the connectivity between the chondrules. This is demonstrated by the systematic decrease in the speed-of-sound from Aba Panu to NWA 869 to Saratov (Table 1).

Lewis et al. [18] used X-ray microtomography (µCT) and scanning electron microscopy to examine the abundance and distribution of porosity in Saratov. They found the porosity of the chondrules to be 1% to 2% by volume, and inferred a porosity of the matrix to be 40 to 60%. The highly porous matrix in Saratov provides only minimal, weak contacts between the chondrules. This is consistent with the low unconfined compressive strength, only 0.97 MPa, and low speed of sound, only 2,350 m/s, measured in Saratov samples.

The ordinary chondrite structure consisting of strong chondrules weakly held together by a minimal amount of matrix appears to be structurally similar to sintered spheres. Love et al [19] performed hypervelocity impact disruptions on four sintered glass sphere targets. None of their targets matched the strength and porosity of Saratov, so they do not provide a direct comparison to Saratov. Their lowest unconfined compressive strength target was 2 MPa, roughly comparable to Saratov, but that sample had a porosity of 60%. They impacted two targets with roughly the same porosity (37% and 39%) which differed in unconfined compressive strength by more than a factor of five (7.9 and 44 MPa), and found their Q^*_C values differed by a factor of two. To explain this difference, they used a result from Horz et al. [20], who

Fig. 4: Plot of log $Q^*_C/S^{0.45}$ vs. log (1 – P).

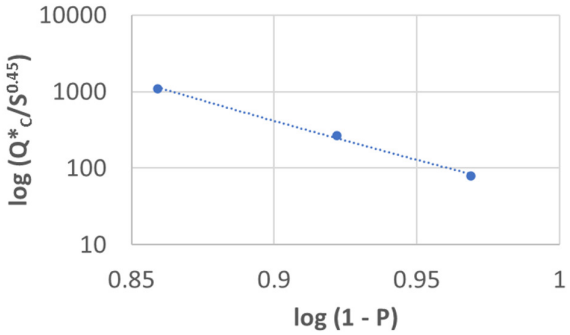

Fig. 5: Plot of log $\beta/S^{0.45}$ vs. log (1 – P).

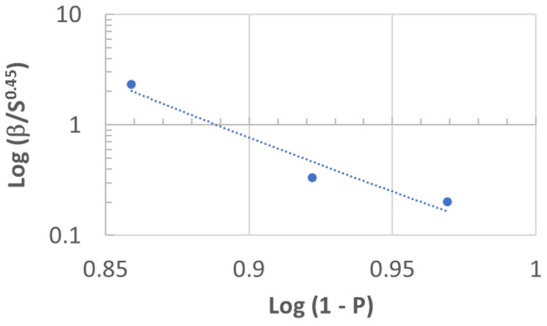

indicated that Q^*_C was proportional to $S^{0.45}$. They found a power law dependence between $Q^*_C/S^{0.45}$ and (1 – P).

Following their approach, we divided the Q^*_C values we determined for each of the three L-chondrites by $S^{0.45}$, and plotted log ($Q^*_C/S^{0.45}$) versus log (1 – P). We followed Love et al. [19] in plotting against (1 – P) since a power law cannot accommodate P = 0. The resulting log-log plot (Figure 4) shows a clear linear trend, with an R^2 value of the fit equal to 0.99. This indicates that, at least for these three L-type ordinary chondrites, which span most of the range of strength and porosity of the L-type ordinary chondrites, the effects of unconfined compressive strength and porosity can be separated. The resulting dependence of Q^*_C on S and P is:

$$Q^*_C = 42.25\ S^{0.45}\ (1 - P)^{-21.7} \qquad \text{(Equation 4)}$$

where Q^*_C is in J/kg for S in MPa.

The β values for these three L-type ordinary chondrites follow the pattern expected from hydrocode modeling, with a progressive decrease in β with increasing porosity. However, β is greater than 2 for each of the three L-type ordinary, indicating that the crater ejecta contributes more momentum to the recoil than the direct transfer of momentum by the impactor, even for the target with the highest porosity. The amount of momentum transferred by the crater ejecta (β - 1) for the two porous meteorite targets, NWA 869 and Saratov, significantly exceeds the modeled values for targets of these porosities and impact speeds [21, 22], although modeling by Bruk Syal et al. [21] gives higher β values for extremely weak targets (cohesive strength = 100 kPa) . Some hydrocode models give (β– 1) <0.4 for targets with porosity like Saratov [22]. These β values exceeding 2 for the porous meteorites are consistent with an earlier measurement of β = 2.1 for highly porous (estimated porosity of 70 to 85% based on measurement of a bulk density of ~0.5 g/cm^3) terrestrial basalt [23].

The mass of the crater ejecta was roughly the same for each of the three types of targets. Since β decreases with increasing porosity, this indicates the mean ejecta velocity decreased with increasing target porosity.

We tested if the same dependence on $S^{0.45}$ might explain the decrease in β with porosity. The plot of log ($\beta/S^{0.45}$) versus log (1 – P) is consistent with a straight line (Figure 5), suggesting that, for these three L-type ordinary chondrite targets, the effects of unconfined compressive strength and porosity on β are also separable. The resulting equation is:

$$\beta = 0.086\ S^{0.45}\ (1 - P)^{-20.8} \qquad \text{(Equation 5)}$$

where S is in MPa. As with the Q^*_C dependance, β shows a very strong dependance on porosity (1 – P), with almost the same exponent as we found for the Q^*_C dependence on (1 – P). This is consistent with results by Holsapple and Housen [24], who also found that β depended strongly on porosity.

The determination of Q^*_F and β allows us to use Equation 1 to determine the maximum change in velocity (ΔV_{max}) that could be imparted by a single kinetic impact without disrupting the target at the 5 km/s impactor speed employed in our experiments. For the low porosity meteorite Aba Panu ΔV_{max} = 1.01 m/s, for the intermediate porosity meteorite NWA 869 ΔV_{max} = 1.32 m/s, and for the high porosity meteorite Saratov ΔV_{max} = 0.61 m/s.

4. Conclusions

Based on hydrocode modeling, Saratov, which has the lowest compressive strength and the highest porosity of the three L-type ordinary chondrites we studied, would be expected to require the highest specific energy, Q^*_C, for the onset of catastrophic disruption. Contrary to this expectation, Saratov has the lowest Q^*_C of these three L-type ordinary chondrite meteorites. The intermediate porosity and intermediate strength meteorite, NWA 869, has the highest Q^*_C of the three meteorites, almost a factor-of-two higher than either Aba Panu or Saratov.

Although the data set is quite limited, these three L-type ordinary chondrites span almost the entire ranges of porosity (P) and unconfined compressive strength (S) reported in the literature for ordinary chondrite meteorites [7]. For these three L-type ordinary chondrites, both Q^*_C and β depend on $S^{0.45}$, as suggested by Horz et al. [20] for lunar rocks. Each shows a very strong dependence on (1 – P), with almost the same exponent in each case, -21.7 for Q^*_C and -20.8 for β. The good correlation of the best fit line indicates that, at least for these three L-type ordinary chondrites, the effects of unconfined compressive strength and porosity can be separated, and that the behavior of Q^*_C and β are both very strongly dependent on sample porosity.

The measured values of β decrease with increasing porosity, as expected from hydrocode modeling. However, β exceeds 2.0 for all three of these L-type ordinary chondrites. This indicates that, in each case, the momentum transferred by the crater ejecta exceeds the direct momentum transfer from the impactor. For both the intermediate porosity NWA 869 and the high porosity Saratov cratering impacts, the momentum enhancement from the crater ejecta is much higher than expected for strong, medium to high porosity targets from hydrocode modeling [21, 22].

The mean crater ejecta mass is approximately the same for each of the three meteorites. Ejecta mass and ejecta speed each affect the recoil. Since the ejecta masses are approximately the same for these three target types, the measured decrease in β indicates that the ejecta speed decreases with increasing porosity. This is consistent with observations by Love at al. [19]. who found a decrease in ejecta speed with increasing target porosity.

The maximum change in velocity that could be imparted by a single kinetic impact without fragmenting the target is within a factor-of-two for these three L-type ordinary chondrites, despite that large differences in porosity and strength. This suggests that simply establishing that a monolithic asteroid is an L-type ordinary chondrite may be sufficient for the design of a deflection mission.

Acknowledgments

This work was funded by a NASA Yearly Opportunity for Research in Planetary Defense grant, #80NSSC22K0241. The NWA 869 measurements were funded by an earlier NASA Solar System Workings grant, #NNX15AM22G. We were assisted in these measurements by Sam Strait, Ian Strait, two Alma College students, Haley Willman and Alexis Rolling and two SUNY-Plattsburgh students, Taylor Pytel and Hunter Wheeler-Cooney. We thank the AVGR crew, C. Cornelison, D. Bowling, F. Perez, A. Parrish, and J. P. Wiens, whose efforts made this project possible.

References

[1] Cheng A. F., Agrusa H. F., Barbee B. W., et al., Momentum transfer from the DART mission kinetic impact on asteroid Dimorphos, Nature (2023), 616,457–460.

[2] Shapiro, I. et al., Defending Planet Earth, National Academies Press (2010) doi:https://doi.org/10.17226/12842.

[3] Flynn, G. J., D. D. Durda, M. M. Strait, R. J. Macke, Limits on Kinetic Impact Deflection of Asteroids from Laboratory Hypervelocity Cratering and Disruption of Meteorites and Analogs**,** HVIS 2022, V001T06A002, https://doi.org/10.1115/HVIS2022-16

[4] Holsapple, K., I. Giblin, K. Housen, A. Nakamura and E. Ryan (2002) Asteroid Impacts: Laboratory Experiments and Scaling Laws, In: *Asteroids III* (eds. W. F. Bottke Jr.,; A. Cellino, P. Paolicchi and R. P. Binzel), University of Arizona Press, 443-462.

[5] Stickle, A., Bruck Syal, M., Cheng, A. F., Collins, G. S., Davison, T. et al.. Benchmarking impact hydrocodes in the strength regime: Implications for modeling deflection by a kinetic impactor. Icarus (2020) 338, pp 113446. ff10.1016/j.icarus.2019.113446ff.

[6] Stickle, A. M. et al. “Effects of Impact and Target Parameters on the Results of a Kinetic Impactor: Predictions for the Double Asteroid Redirection Test (DART) Mission” *Planet. Sci. J.*, 3:248 (2022), 29 pp. https://doi.org/10.3847/PSJ/ac91cc

[7] Flynn, G. J., G. J. Consolmagno, P. Brown, R. J. Macke (2018) Physical properties of the stone meteorites: Implications for the properties of their parent bodies, Geochemistry, 78**,** 269-298.

[8] D. Ostrowski and K. Bryson (2020) Laboratory examination of the physical properties of ordinary chondrites, Meteoritics & Planetary Science 55, 2007–2020.

[9] Slyuta, E.N., S. M. Nikitin, A. V. Korochantsev, and C. A. Lorents (2008) Physical and mechanical properties of Sayh al Uhaymir 001 and Ghubara meteorites, Lunar and Planetary Science Conference XXXIX (2008) Abstract #1056.

[10] Macke R. J., Britt D. T. and Consolmagno G. J “New pycnometer design for thin-sliced meteorites” *Lunar and Planetary Science Conference XLIV* (2013) Abstract #1398).

[11] Macke R. J., Kent J. J., Kiefer W. S. and Britt D. T. “3D-Laser-Scanning Technique Applied to Bulk Density Measurements of Apollo Lunar Samples,” Lunar and *Planetary Science Conference XLVI* ((2015) Abstract #1716.

[12] Cotto-Figueroa, D. et al. “On the Strength of the Aba Panu (L3) Meteorite: Implications for Hazard Mitigation” *Lunar and Planetary Science Conference LI* (2020) Abstract #2646.

[13] Pytel, T. et a. (2023) Speed-of-sound Measurements on Meteorite samples, 54th Lunar and Planetary Science Conference, LPI Contrib. No. 2806, Abstract# 1246.
[14] Flynn, G. J. (2004) Physical properties of meteorites and interplanetary dust particles: clues to the properties of meteorite and their parent bodies" Earth Moon Planets 95, 361-374
[15] Karcz, J. et al. "The Ames Vertical Gun Range" Lunar and Planetary Science Conference XLVII (2016) Abstract #2599.
[16] Flynn, G. J. et al. (2018) Hypervelocity cratering and disruption of the Northwest Africa 869 ordinary chondrite meteorite: Implications for crater production, catastrophic disruption, momentum transfer and dust production on asteroids, *Planetary and Space Science*, 164, 91-105.
[17] Fujiwara, A. et al. (1989) Experiments and Scaling Laws for Catastrophic Collisions (1989) in *Asteroids II (eds.:* R. P. Binzel, T. Gehrels, and M. S. Matthews), University of Arizona Press, Tucson, 240-265.
[18] Lewis et al. (2018) Chondrule porosity in the L4 chondrite Saratov: Dissolution, chemical transport, and fluid flow Geochimica et Cosmochimica Acta, Volume 240, 293-313.
[19] Love, S. G., F. Horz, and D. E. Brownlee (1993) Target Porosity Effects in Impact Cratering and Collisional Disruption, Icarus, 105, 216-224. spheres.
[20] Horz, F. et al. (1975) Catastrophic Rupture of Lunar Rocks: A Monte Carlo Simulation, The Moon, 13, 235-258.
[21] Bruck Syal, M., J. M. Owen, and P. L. Miller (2016) Deflection by kinetic impact: Sensitivity to asteroid properties, *Icarus*, 269, 50-61.
[22] Jutzi, M. and P. Michel (2014) Hypervelocity impacts on asteroids and momentum transfer I. Numerical simulations using porous targets, Icarus, 229, 247-253.
[23] Flynn, G. J. et al. (2015) Hypervelocity Cratering and Disruption of Porous Pumice Targets: Implications for Crater Production, Catastrophic Disruption, and Momentum Transfer on Porous Asteroids, Planetary and Space Science, 107, 64-76.
[24] Holsapple, K. A., Housen, K. R. (2013) Mitigation by Impacts: Theory, experiments, and code calculations https://iaaspace.org/wp-content/uploads/iaa/Scientific%20Activity/conf/pdc2013/IAA-PDC13-04-04.pdf

9th IAA Planetary Defense Conference – PDC 2025
5-9 May 2025, Stellenbosch, Cape Town, South Africa

IAA-PDC-25-06-52

HYPERVELOCITY CRATERING AND DISRUPTION OF THREE L-TYPE ORDINARY CHONDRITES: EFFECTS OF STRENGTH AND POROSITY ON DISRUPTION ENERGY

George J. Flynn[1], Melissa Strait[2], Daniel D. Durda[3], and Robert Macke[4]
[1]*SUNY-Plattsburgh, 101 Broad St., Plattsburgh NY 12901 USA (george.flynn@plattsburgh.edu),*
[2]*Alma College, Alma, MI 48801 (straitm@alma.edu),*
[3]*Southwest Research Institute, 1301 Walnut Street, Suite 400, Boulder CO 80302 (durda@boulder.swri.edu),*
[4]*Vatican Observatory, V-00120 Vatican City(macke@jesuits.net)*

Abstract

The response of asteroids to hypervelocity impact influences momentum transfer in cratering and fragmentation in disruptive collisions, which together limit the maximum change in velocity (ΔV_{MAX}) that can be imparted by a single kinetic impact. For Q_F, the energy per unit target mass for onset of fragmentation, β, the ratio of impactor momentum to momentum acquired by the target, and v_i, the impactor mass: $\Delta V_{MAX} = 2Q_F\beta/v_i$. Hydrocode modeling indicates β decreases with increasing target porosity, and, Q^*_C, the energy for the onset of catastrophic disruption, increases with increasing target porosity or decreasing target strength. To test this, we performed hypervelocity cratering and disruption experiments on three asteroid samples of similar compositions but different porosities (P) and compressive strengths (S): the low porosity L3 Ordinary Chondrite (OC) meteorite Aba Panu (P ~3.1%, S = 438 MPa), the intermediate porosity L3-6 OC Northwest Africa 869 (NWA 869) (P ~7.8%, S = 87 MPa), and the high porosity L4 OC Saratov (P ~14.1%, S = 0.97 MPa). β followed the pattern expected from modeling: β = 3.5 for Aba Panu, 2.7 for NWA 869, and 2.5 for Saratov. However, the decrease in β with increasing porosity is not as strong as suggested by hydrocode modeling. The energy required for catastrophic disruption (Q^*_C) deviated from modeling that indicates more porous targets should be more resistant to disruption. Saratov gave Q^*_C = 1,090 J/kg, comparable to the low-porosity OC Aba Panu (Q^*_C = 1,230 J/kg) but much lower than the 1,990 J/kg we measured for the intermediate porosity OC NWA 869. Earlier work by other investigators proposed that for disruptive events Q^*_C is proportional $S^{0.45}$. Using this approach, we found a power law behavior between $Q^*_C/S^{0.45}$ and (1 – P), indicating that, for these three L-type OCs, the dependence of Q^*_C on strength can be separated from the dependence on porosity. Further, we determined Q^*_F, the energy per unit target mass for the onset of fragmentation, and calculated ΔV_{MAX}, for each ordinary chondrite There is only a small difference between ΔV_{MAX} values for these three meteorites vary, which vary from 0.61 to 1.32 m/s, compared to the factor-of-seven difference we reported between NWA 869 and the anhydrous carbonaceous chondrite Northwest Africa 4502. This suggests remote sensing demonstrating an asteroid is similar to an L-type OC may be sufficient for selecting the impactor mass and speed for a kinetic impact deflection that avoids significant fragmentation.

Keywords: Hypervelocity Impact Cratering, Hypervelocity Impact Fragmentation, Meteorites, Ordinary Chondrites, Kinetic Impact Deflection

1. Introduction

Kinetic impact deflection, which was demonstrated by the NASA Double Asteroid Redirection Test (DART) spacecraft [1], is regarded as the most mature technology currently available for deflection of a monolithic asteroid up to a few hundred meters in diameter that is on a collision course with the Earth [2]. However, a successful kinetic impact deflection requires a knowledge of the momentum added by the impact or sequence of impacts as well as the maximum kinetic energy that can be deposited in the target without fragmentation, since this could leave a fragment of the target on a collision course with the Earth.

The momentum transferred to a monolithic rock target in a hypervelocity kinetic impact is observed to be greater than the original momentum of the projectile because of the ejection of cratering debris in a direction approximately opposite to the flight direction of the projectile. In a cratering impact on a monolithic target the recoil momentum has contributions from two factors:

1) the momentum of the impactor, and,
2) the momentum provided by the crater ejecta.

The total momentum transferred in a cratering impact is characterized by a factor β, which is the ratio of the increase in momentum of the target to the momentum of the projectile, where:

$$\beta = 1 + p_e/p_i \qquad \text{(Equation 1)}$$

where p_e is the momentum of the crater ejecta and p_i is the impactor momentum. So, β is 1 in the absence of crater ejecta and (β -1) is the momentum enhancement from the crater ejecta.

To avoid fragmentation, which could leave a large piece of the target asteroid on a collision course with Earth, the maximum change in velocity, ΔV_{max}, that can be achieved in a single kinetic impact is restricted by the requirement:

$$\Delta V_{max} = 2\ \beta\ Q^*_F/v_i \qquad \text{(Equation 2)}$$

where Q^*_F is the energy per unit target mass where the outcome of an impact transitions from cratering to fragmentation, and v_i is the speed of the impactor relative to the asteroid [3]. Thus, both β and Q^*_F must be known for the asteroid in question in order to design a successful kinetic impact deflection mission.

Modeling of hypervelocity impacts has provided insights into the expected dependance of collisional outcomes, particularly β and Q^*_F, on the strength and porosity of the target asteroid. Compaction of porous material is expected to help absorb the impact energy and reduce the transmission of shock, localizing much of the damage to the immediate region of the impact [4]. The impact modeling generally indicates that lower strength and/or higher porosity increases the collisional survival of a monolithic asteroid by requiring a higher energy for fragmentation [5, 6]. However, most of this modeling employs the physical properties of terrestrial rocks.

Asteroids span a wide diversity of mineralogical compositions, porosities, and strengths. Stickle et al. [5, 6] showed that the two most important physical properties

of the target affecting the modeled outcome of hypervelocity impact are the target strength and the target porosity. Thus, a knowledge of the strength, porosity, and likely the mineralogical composition of the target asteroid are each critical in insuring a successful kinetic impact deflection. The mineralogical composition of an asteroid can be determined remotely by reflection spectroscopy using terrestrial or space-based telescopes. However, the porosity of an asteroid is usually determined by gravitational perturbation. This requires either another relatively nearby, large asteroid or a flyby spacecraft. A strength determination generally requires a lander spacecraft to sample and test the underlying bedrock.

Meteorites provide laboratory samples of their asteroidal parent bodies, allowing measurement of the porosity and strength of samples of a variety of asteroid parent bodies. The recovered meteorites provide direct evidence for the diversity of mineralogies, strengths, and porosities among the Near-Earth Objects (NEOs). However, the weakest meteors fragment so severely during atmospheric deceleration that this group is not well sampled by the meteorites since only dust survives.

The recovered meteorites range from the weak, highly porous CI1 carbonaceous chondrites like Orgueil to the strong, low porosity iron meteorites like Canyon Diablo. The types and relative frequencies of meteorite falls provide some indication of the mineralogy, porosity, and strength range of the population of NEOs. The recovery of observed meteorite falls provides an indication of the relative abundance of each type in near-Earth space. Iron meteorites constitute less than 4% of all falls, stony-iron meteorites about 1.0%, and stony meteorites about 95%.

The ordinary chondrites are the most common stony meteorites that fall to Earth. Among the ordinary chondrites, there are three distinct types based on their mineralogies: the high-iron or H-type, the low-iron or L-type, and the very low iron or LL-type. The physical properties, including the mineralogies, the porosities, and the compressional and tensile strengths, of the stone meteorites, which constitute about 95% of all meteorite falls, were summarized in reviews by Flynn et al. [7] and Ostrowski and Bryson [8]. These reviews are consistent with the observation of Slyuta et al. [9] that: “There are no analogues among terrestrial igneous and sedimentary rocks and ores… [for the] set of physical and mechanical properties of the meteorites.” Slyuta et al. [9] indicated that knowledge of meteorite or meteorite-analog physical properties is critical to estimating the hazard of asteroidal impacts, creating engineering models for asteroid sample collection, and understanding the requirements for asteroid deflection.

2. Samples

To characterize the response of asteroid material to hypervelocity impacts we performed hypervelocity impact cratering and disruption experiments on three L-type ordinary chondrite meteorites, Aba Panu, Northwest Africa 869 (NWA 869), and Saratov. Since all three a L-type ordinary chondrites, they have very similar mineralogies, and thus similar remote sensing spectra. These three L-type meteorites were selected for our study because they were minimally weathered by exposure on the Earth, they were not severely shocked during residence near the surface and during ejection from their parent bodies, and they were available in sufficient quantity and size for the experiments. These three L-type ordinary chondrites span most of the strength range and much of the porosity range of the ordinary chondrite meteorites.

Table 1: Physical Properties and Impact Outcomes for three L-type Meteorites.

Meteorite	Type	Porosity (%)	Comp. Strength (MPa)	Speed of Sound (m/s)	β	Q^*_C J/kg)	Q^*_F (J/kg)	ΔV_{max} at ~5 km/s
Aba Panu	L3	3.1	438	5,100	3.7	1,230	680	1.01
NWA 869	L3-6	7.8	87	3,280	2.5	1,990	1320	1.32
Saratov	L4	14.1	0.97	2,350	2.3	1,090	660	0.61

We performed physical properties measurements, including the bulk and grain densities, allowing determination of the porosity, the unconfined compressive strength, the speed of sound, and Young's modulus on each of the three meteorites (Table 1). The grain volume was determined using Ideal Gas Pycnometry and the bulk volume was determined by laser scanning to target, as described by Macke et al. [10, 11]. These values were used to determine the grain density (ρ_g) and the bulk density (ρ_b) of each target type. The target porosity (P) was then determined using:

$$P = 1 - \rho_b/\rho_g \qquad \text{(Equation 3)}$$

The unconfined compressive strengths of NWA 869 and of Saratov were measured on 1 cm cubes of each meteorite by applying a pressure across two opposite faces of each cube using a hydraulic press to slowly increase the pressure until failure occurred. The strength of Aba Panu is from Cotto-Figueroa et al. [12] The speed of sound of Aba Panu and NWA 869 were measured using an ultrasonic thickness gauge in a mode that determines the sound speed when the sample thickness is known [13]. The speed of sound of Saratov samples was determined in earlier work [14].

These three L-type ordinary chondrites selected for our measurements span most of the range of porosity, and strength of the ordinary chondrite meteorites.

Aba Panu is a low porosity L3 ordinary chondrite. It is a fresh fall, having a low degree of terrestrial weathering (W0), but is somewhat shocked (S4).

NWA 869 is an intermediate porosity, brecciated L3-6 ordinary chondrite. NWA 869 is a find, but it experienced a low degree of terrestrial weathering (W1) and lesser shock (S3) than Aba Panu.

Saratov is a high porosity L4 ordinary chondrite. It is an observed fall having a low degree of terrestrial weathering (W0), but is somewhat shocked (S4).

2. Hypervelocity Impact Experiments

We conducted hypervelocity impact cratering and disruption measurements at the NASA Ames Vertical Gun Range (AVGR). Each target was suspended from the ceiling of the sample chamber on an ~2 m long fishing line. This allowed the targets to recoil freely in cratering experiments and did not interfere with the disruption in fragmentation experiments. The sample chamber was pumped to ~0.5 torr to minimize atmospheric interference with the projectile. The impactors were solid aluminum spheres having diameters of 1/16", 1/8", or 1/4" aimed at the center of each target. The speed of each impactor was determined using a laser-interrupt system. The impactor speeds ranged from 4.0 to 5.8 km/s. The AVGR and its gun chamber are described in detail by Karz et al. [15]. Some of the hypervelocity cratering and disruption results for the NWA 869

meteorite were described in an earlier paper [16], which includes a complete description of the experimental setup employed for these measurements.

For the fragmentation impacts all of the target material was recovered from the gun chamber after each impact. The mass of the largest fragment produced in the impact, M_L, was compared to the initial mass of the target, M_T. Since no two individual rocks, even from the same material, are identical in flaw distribution, shape, etc., the energy required for fragmentation is usually determined from the outcomes of a series of impacts conducted at different impactor specific energies, Q*, the impactor kinetic energy per unit target mass [17]. The energy for the onset of catastrophic disruption Q^*_C, is determined from a plot of M_L/M_T vs. Q* [17]. Q^*_C is generally regarded as the impactor energy where the mass of the largest fragment produced in the impact is one-half the target mass. Q^*_C is the value of Q* where a horizontal line at $M_L/M_T = 0.5$ intersects the best fit line to the fragmentation data (Figure 1). To determine Q^*_F, the energy for the onset of fragmentation, we extended the best fit line for M_L/M_T vs Q* to the point where it intersected $M_L/M_T = 0.98$, which corresponds to a cratering impact.

Figure 1: M_L/M_T vs Q* for Aba Panu.

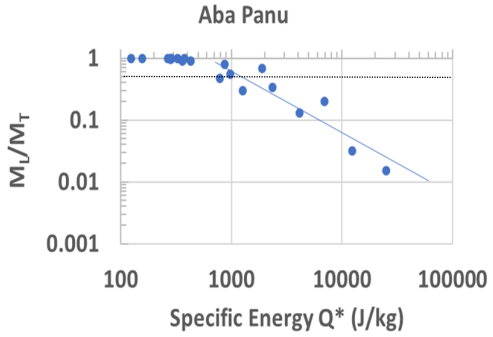

Figure 2: M_L/M_T vs Q* for NWA 869.

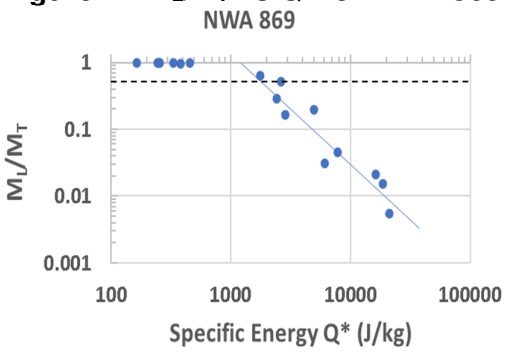

Figure 3: M_L/M_T vs Q* for Saratov.

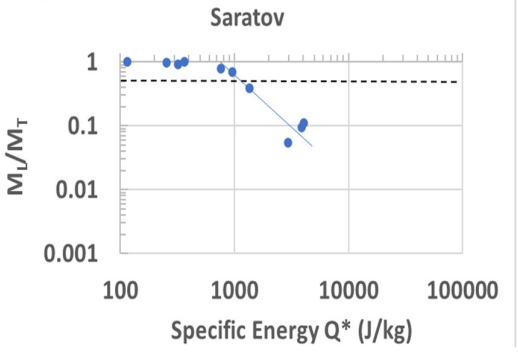

We performed ten fragmentation impacts on Aba Panu at specific energies ranging from 791 J/kg to 24,901 J/kg. These impacts gave M_L/M_T values ranging from 0.015 to 0.806 (Figure 1). The best fit line to this data set gives Q^*_C =1,230 J/kg and Q^*_F = 680 J/kg. The ten fragmentation impacts on NWA 869 were conducted at energies ranging from 1,764 J/kg to 21,225 J/kg resulting in M_L/M_T values ranging from 0.016 to 0.639 (Figure 2). The best fit line to these impacts gives Q^*_C =1,990 J/kg and Q^*_F = 1,320 J/kg. Seven fragmentation impacts were performed on Saratov at specific energies ranging from 708 J/kg to 4,069 J/kg resulting in M_L/M_T values ranging from 0.055 to 0.889 (Figure 3). The best fit line to these impacts gives Q^*_C =1,090 J/kg and Q^*_F = 660 J/kg.

For each cratering experiment marked grids were placed below and behind each target. A high-speed video camera was placed above the target and second high-speed video camera was placed in front of the target to record each impact. The resulting target recoil speed was determined from the target motion relative to the grids in a sequence of frames taken after each impact. From this recoil speed, the target

mass, and the impactor mass and speed we determined the value of β. We also determined the mass of the crater ejecta (M_T - M_L), measured the depth and the diameter of the crater, and determined the shape of the crater. The speeds of some of the larger ejecta fragments were also determined to ensure consistency between the measured recoil speed and the momentum carried by the crater ejecta. On the plots of M_L/M_T vs Q* these cratering impacts scatter around a horizontal line near M_L/M_T = 0.98 (Figures 1, 2, and 3)).

We performed ten cratering experiments on Aba Panu at specific energies ranging from 124 J/kg to 430 J/kg (Figure 1). These impacts gave a value of β = 3.7. The mass of the crater ejecta ranged from 1 g to 5 g. with a mean of 2.8 g. We performed seven cratering experiments on NWA 869 at specific energies ranging from 165 J/kg to 460 J/kg (Figure 2). These impacts gave a value of β = 2.5. The mass of the crater ejecta ranged from <0.5 g to 5 g. with a mean of 2.6 g. We performed four cratering experiments on NWA 869 at specific energies ranging from 115 J/kg to 363 J/kg (Figure 3). These impacts gave a value of β = 2.3. The mass of the crater ejecta ranged from 2 g to 3 g. with a mean of 2.3 g. The craters in Aba Panu and NWA 869 were approximately bowl shaped with depths approximately one-half their diameters. The craters in Saratov were more elongated, approximating a cylindrical shape.

3. Discussion

Saratov has the lowest compressive strength and the highest porosity of any of these three, L-type ordinary chondrites we measured. Based on hydrocode modeling, Saratov was expected to be the most resistant of the three L-type ordinary chondrites to fragmentation or disruption (i.e., have highest Q^*_F and Q^*_C). However, Saratov had the lowest Q^*_F and Q^*_C of these three meteorites.

The ordinary chondrite meteorites have a two-component structure: strong, low porosity chondrules consisting of crystalline olivine or pyroxene, embedded in a weaker, more porous matrix. The increase in porosity generally corresponds to an increase in the matrix porosity, leaving larger pore spaces that result in a decrease in the connectivity between the chondrules. This is demonstrated by the systematic decrease in the speed-of-sound from Aba Panu to NWA 869 to Saratov (Table 1).

Lewis et al. [18] used X-ray microtomography (µCT) and scanning electron microscopy to examine the abundance and distribution of porosity in Saratov. They found the porosity of the chondrules to be 1% to 2% by volume, and inferred a porosity of the matrix to be 40 to 60%. The highly porous matrix in Saratov provides only minimal, weak contacts between the chondrules. This is consistent with the low unconfined compressive strength, only 0.97 MPa, and low speed of sound, only 2,350 m/s, measured in Saratov samples.

The ordinary chondrite structure consisting of strong chondrules weakly held together by a minimal amount of matrix appears to be structurally similar to sintered spheres. Love et al [19] performed hypervelocity impact disruptions on four sintered glass sphere targets. None of their targets matched the strength and porosity of Saratov, so they do not provide a direct comparison to Saratov. Their lowest unconfined compressive strength target was 2 MPa, roughly comparable to Saratov, but that sample had a porosity of 60%. They impacted two targets with roughly the same porosity (37% and 39%) which differed in unconfined compressive strength by more than a factor of five (7.9 and 44 MPa), and found their Q^*_C values differed by a factor of two. To explain this difference, they used a result from Horz et al. [20], who

Fig. 4: Plot of log $Q^*_C/S^{0.45}$ vs. log (1 – P).

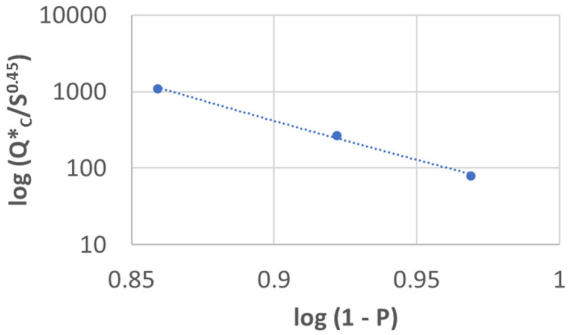

Fig. 5: Plot of log $\beta/S^{0.45}$ vs. log (1 – P).

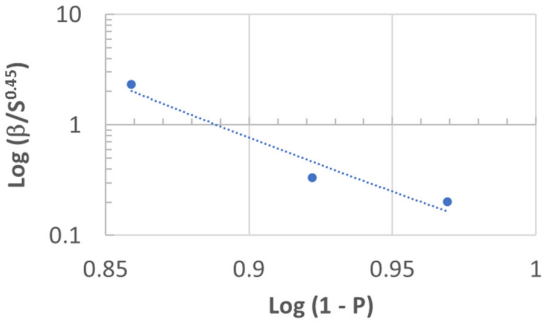

indicated that Q^*_C was proportional to $S^{0.45}$. They found a power law dependence between $Q^*_C/S^{0.45}$ and (1 – P).

Following their approach, we divided the Q^*_C values we determined for each of the three L-chondrites by $S^{0.45}$, and plotted log ($Q^*_C/S^{0.45}$) versus log (1 – P). We followed Love et al. [19] in plotting against (1 – P) since a power law cannot accommodate P = 0. The resulting log-log plot (Figure 4) shows a clear linear trend, with an R^2 value of the fit equal to 0.99. This indicates that, at least for these three L-type ordinary chondrites, which span most of the range of strength and porosity of the L-type ordinary chondrites, the effects of unconfined compressive strength and porosity can be separated. The resulting dependence of Q^*_C on S and P is:

$$Q^*_C = 42.25\ S^{0.45}\ (1 - P)^{-21.7} \qquad \text{(Equation 4)}$$

where Q^*_C is in J/kg for S in MPa.

The β values for these three L-type ordinary chondrites follow the pattern expected from hydrocode modeling, with a progressive decrease in β with increasing porosity. However, β is greater than 2 for each of the three L-type ordinary, indicating that the crater ejecta contributes more momentum to the recoil than the direct transfer of momentum by the impactor, even for the target with the highest porosity. The amount of momentum transferred by the crater ejecta (β - 1) for the two porous meteorite targets, NWA 869 and Saratov, significantly exceeds the modeled values for targets of these porosities and impact speeds [21, 22], although modeling by Bruk Syal et al. [21] gives higher β values for extremely weak targets (cohesive strength = 100 kPa) . Some hydrocode models give (β– 1) <0.4 for targets with porosity like Saratov [22]. These β values exceeding 2 for the porous meteorites are consistent with an earlier measurement of β = 2.1 for highly porous (estimated porosity of 70 to 85% based on measurement of a bulk density of ~0.5 g/cm^3) terrestrial basalt [23].

The mass of the crater ejecta was roughly the same for each of the three types of targets. Since β decreases with increasing porosity, this indicates the mean ejecta velocity decreased with increasing target porosity.

We tested if the same dependence on $S^{0.45}$ might explain the decrease in β with porosity. The plot of log ($\beta/S^{0.45}$) versus log (1 – P) is consistent with a straight line (Figure 5), suggesting that, for these three L-type ordinary chondrite targets, the effects of unconfined compressive strength and porosity on β are also separable. The resulting equation is:

$$\beta = 0.086\ S^{0.45}\ (1 - P)^{-20.8} \qquad \text{(Equation 5)}$$

where S is in MPa. As with the Q^*_C dependance, β shows a very strong dependance on porosity (1 – P), with almost the same exponent as we found for the Q^*_C dependence on (1 – P). This is consistent with results by Holsapple and Housen [24], who also found that β depended strongly on porosity.

The determination of Q^*_F and β allows us to use Equation 1 to determine the maximum change in velocity (ΔV_{max}) that could be imparted by a single kinetic impact without disrupting the target at the 5 km/s impactor speed employed in our experiments. For the low porosity meteorite Aba Panu ΔV_{max} = 1.01 m/s, for the intermediate porosity meteorite NWA 869 ΔV_{max} = 1.32 m/s, and for the high porosity meteorite Saratov ΔV_{max} = 0.61 m/s.

4. Conclusions

Based on hydrocode modeling, Saratov, which has the lowest compressive strength and the highest porosity of the three L-type ordinary chondrites we studied, would be expected to require the highest specific energy, Q^*_C, for the onset of catastrophic disruption. Contrary to this expectation, Saratov has the lowest Q^*_C of these three L-type ordinary chondrite meteorites. The intermediate porosity and intermediate strength meteorite, NWA 869, has the highest Q^*_C of the three meteorites, almost a factor-of-two higher than either Aba Panu or Saratov.

Although the data set is quite limited, these three L-type ordinary chondrites span almost the entire ranges of porosity (P) and unconfined compressive strength (S) reported in the literature for ordinary chondrite meteorites [7]. For these three L-type ordinary chondrites, both Q^*_C and β depend on $S^{0.45}$, as suggested by Horz et al. [20] for lunar rocks. Each shows a very strong dependence on (1 – P), with almost the same exponent in each case, -21.7 for Q^*_C and -20.8 for β. The good correlation of the best fit line indicates that, at least for these three L-type ordinary chondrites, the effects of unconfined compressive strength and porosity can be separated, and that the behavior of Q^*_C and β are both very strongly dependent on sample porosity.

The measured values of β decrease with increasing porosity, as expected from hydrocode modeling. However, β exceeds 2.0 for all three of these L-type ordinary chondrites. This indicates that, in each case, the momentum transferred by the crater ejecta exceeds the direct momentum transfer from the impactor. For both the intermediate porosity NWA 869 and the high porosity Saratov cratering impacts, the momentum enhancement from the crater ejecta is much higher than expected for strong, medium to high porosity targets from hydrocode modeling [21, 22].

The mean crater ejecta mass is approximately the same for each of the three meteorites. Ejecta mass and ejecta speed each affect the recoil. Since the ejecta masses are approximately the same for these three target types, the measured decrease in β indicates that the ejecta speed decreases with increasing porosity. This is consistent with observations by Love at al. [19]. who found a decrease in ejecta speed with increasing target porosity.

The maximum change in velocity that could be imparted by a single kinetic impact without fragmenting the target is within a factor-of-two for these three L-type ordinary chondrites, despite that large differences in porosity and strength. This suggests that simply establishing that a monolithic asteroid is an L-type ordinary chondrite may be sufficient for the design of a deflection mission.

Acknowledgments

This work was funded by a NASA Yearly Opportunity for Research in Planetary Defense grant, #80NSSC22K0241. The NWA 869 measurements were funded by an earlier NASA Solar System Workings grant, #NNX15AM22G. We were assisted in these measurements by Sam Strait, Ian Strait, two Alma College students, Haley Willman and Alexis Rolling and two SUNY-Plattsburgh students, Taylor Pytel and Hunter Wheeler-Cooney. We thank the AVGR crew, C. Cornelison, D. Bowling, F. Perez, A. Parrish, and J. P. Wiens, whose efforts made this project possible.

References

[1] Cheng A. F., Agrusa H. F., Barbee B. W., et al., Momentum transfer from the DART mission kinetic impact on asteroid Dimorphos, Nature (2023), 616,457–460.

[2] Shapiro, I. et al., Defending Planet Earth, National Academies Press (2010) doi:https://doi.org/10.17226/12842.

[3] Flynn, G. J., D. D. Durda, M. M. Strait, R. J. Macke, Limits on Kinetic Impact Deflection of Asteroids from Laboratory Hypervelocity Cratering and Disruption of Meteorites and Analogs**,** HVIS 2022, V001T06A002, https://doi.org/10.1115/HVIS2022-16

[4] Holsapple, K., I. Giblin, K. Housen, A. Nakamura and E. Ryan (2002) Asteroid Impacts: Laboratory Experiments and Scaling Laws, In: *Asteroids III* (eds. W. F. Bottke Jr.,; A. Cellino, P. Paolicchi and R. P. Binzel), University of Arizona Press, 443-462.

[5] Stickle, A., Bruck Syal, M., Cheng, A. F., Collins, G. S., Davison, T. et al.. Benchmarking impact hydrocodes in the strength regime: Implications for modeling deflection by a kinetic impactor. Icarus (2020) 338, pp 113446. ff10.1016/j.icarus.2019.113446ff.

[6] Stickle, A. M. et al. “Effects of Impact and Target Parameters on the Results of a Kinetic Impactor: Predictions for the Double Asteroid Redirection Test (DART) Mission” *Planet. Sci. J.*, 3:248 (2022), 29 pp. https://doi.org/10.3847/PSJ/ac91cc

[7] Flynn, G. J., G. J. Consolmagno, P. Brown, R. J. Macke (2018) Physical properties of the stone meteorites: Implications for the properties of their parent bodies, Geochemistry, 78**,** 269-298.

[8] D. Ostrowski and K. Bryson (2020) Laboratory examination of the physical properties of ordinary chondrites, Meteoritics & Planetary Science 55, 2007–2020.

[9] Slyuta, E.N., S. M. Nikitin, A. V. Korochantsev, and C. A. Lorents (2008) Physical and mechanical properties of Sayh al Uhaymir 001 and Ghubara meteorites, Lunar and Planetary Science Conference XXXIX (2008) Abstract #1056.

[10] Macke R. J., Britt D. T. and Consolmagno G. J “New pycnometer design for thin-sliced meteorites” *Lunar and Planetary Science Conference XLIV* (2013) Abstract #1398).

[11] Macke R. J., Kent J. J., Kiefer W. S. and Britt D. T. “3D-Laser-Scanning Technique Applied to Bulk Density Measurements of Apollo Lunar Samples,” Lunar and *Planetary Science Conference XLVI* ((2015) Abstract #1716.

[12] Cotto-Figueroa, D. et al. “On the Strength of the Aba Panu (L3) Meteorite: Implications for Hazard Mitigation” *Lunar and Planetary Science Conference LI* (2020) Abstract #2646.

[13] Pytel, T. et a. (2023) Speed-of-sound Measurements on Meteorite samples, 54th Lunar and Planetary Science Conference, LPI Contrib. No. 2806, Abstract# 1246.
[14] Flynn, G. J. (2004) Physical properties of meteorites and interplanetary dust particles: clues to the properties of meteorite and their parent bodies" Earth Moon Planets 95, 361-374
[15] Karcz, J. et al. "The Ames Vertical Gun Range" Lunar and Planetary Science Conference XLVII (2016) Abstract #2599.
[16] Flynn, G. J. et al. (2018) Hypervelocity cratering and disruption of the Northwest Africa 869 ordinary chondrite meteorite: Implications for crater production, catastrophic disruption, momentum transfer and dust production on asteroids, *Planetary and Space Science*, 164, 91-105.
[17] Fujiwara, A. et al. (1989) Experiments and Scaling Laws for Catastrophic Collisions (1989) in *Asteroids II (eds.:* R. P. Binzel, T. Gehrels, and M. S. Matthews), University of Arizona Press, Tucson, 240-265.
[18] Lewis et al. (2018) Chondrule porosity in the L4 chondrite Saratov: Dissolution, chemical transport, and fluid flow Geochimica et Cosmochimica Acta, Volume 240, 293-313.
[19] Love, S. G., F. Horz, and D. E. Brownlee (1993) Target Porosity Effects in Impact Cratering and Collisional Disruption, Icarus, 105, 216-224. spheres.
[20] Horz, F. et al. (1975) Catastrophic Rupture of Lunar Rocks: A Monte Carlo Simulation, The Moon, 13, 235-258.
[21] Bruck Syal, M., J. M. Owen, and P. L. Miller (2016) Deflection by kinetic impact: Sensitivity to asteroid properties, *Icarus*, 269, 50-61.
[22] Jutzi, M. and P. Michel (2014) Hypervelocity impacts on asteroids and momentum transfer I. Numerical simulations using porous targets, Icarus, 229, 247-253.
[23] Flynn, G. J. et al. (2015) Hypervelocity Cratering and Disruption of Porous Pumice Targets: Implications for Crater Production, Catastrophic Disruption, and Momentum Transfer on Porous Asteroids, Planetary and Space Science, 107, 64-76.
[24] Holsapple, K. A., Housen, K. R. (2013) Mitigation by Impacts: Theory, experiments, and code calculations https://iaaspace.org/wp-content/uploads/iaa/Scientific%20Activity/conf/pdc2013/IAA-PDC13-04-04.pdf

9th IAA Planetary Defense Conference – PDC 2025
5-9 May 2025, Stellenbosch, Cape Town, South Africa

IAA-PDC-25-06-52

HYPERVELOCITY CRATERING AND DISRUPTION OF THREE L-TYPE ORDINARY CHONDRITES: EFFECTS OF STRENGTH AND POROSITY ON DISRUPTION ENERGY

George J. Flynn[1], Melissa Strait[2], Daniel D. Durda[3], and Robert Macke[4]
[1]*SUNY-Plattsburgh, 101 Broad St., Plattsburgh NY 12901 USA (george.flynn@plattsburgh.edu),*
[2]*Alma College, Alma, MI 48801 (straitm@alma.edu),*
[3]*Southwest Research Institute, 1301 Walnut Street, Suite 400, Boulder CO 80302 (durda@boulder.swri.edu),*
[4]*Vatican Observatory, V-00120 Vatican City(macke@jesuits.net)*

Abstract

The response of asteroids to hypervelocity impact influences momentum transfer in cratering and fragmentation in disruptive collisions, which together limit the maximum change in velocity (ΔV_{MAX}) that can be imparted by a single kinetic impact. For Q_F, the energy per unit target mass for onset of fragmentation, β, the ratio of impactor momentum to momentum acquired by the target, and v_i, the impactor mass: $\Delta V_{MAX} = 2Q_F\beta/v_i$. Hydrocode modeling indicates β decreases with increasing target porosity, and, Q^*_C, the energy for the onset of catastrophic disruption, increases with increasing target porosity or decreasing target strength. To test this, we performed hypervelocity cratering and disruption experiments on three asteroid samples of similar compositions but different porosities (P) and compressive strengths (S): the low porosity L3 Ordinary Chondrite (OC) meteorite Aba Panu (P ~3.1%, S = 438 MPa), the intermediate porosity L3-6 OC Northwest Africa 869 (NWA 869) (P ~7.8%, S = 87 MPa), and the high porosity L4 OC Saratov (P ~14.1%, S = 0.97 MPa). β followed the pattern expected from modeling: β = 3.5 for Aba Panu, 2.7 for NWA 869, and 2.5 for Saratov. However, the decrease in β with increasing porosity is not as strong as suggested by hydrocode modeling. The energy required for catastrophic disruption (Q^*_C) deviated from modeling that indicates more porous targets should be more resistant to disruption. Saratov gave Q^*_C = 1,090 J/kg, comparable to the low-porosity OC Aba Panu (Q^*_C = 1,230 J/kg) but much lower than the 1,990 J/kg we measured for the intermediate porosity OC NWA 869. Earlier work by other investigators proposed that for disruptive events Q^*_C is proportional $S^{0.45}$. Using this approach, we found a power law behavior between $Q^*_C/S^{0.45}$ and (1 – P), indicating that, for these three L-type OCs, the dependence of Q^*_C on strength can be separated from the dependence on porosity. Further, we determined Q^*_F, the energy per unit target mass for the onset of fragmentation, and calculated ΔV_{MAX}, for each ordinary chondrite There is only a small difference between ΔV_{MAX} values for these three meteorites vary, which vary from 0.61 to 1.32 m/s, compared to the factor-of-seven difference we reported between NWA 869 and the anhydrous carbonaceous chondrite Northwest Africa 4502. This suggests remote sensing demonstrating an asteroid is similar to an L-type OC may be sufficient for selecting the impactor mass and speed for a kinetic impact deflection that avoids significant fragmentation.

Keywords: Hypervelocity Impact Cratering, Hypervelocity Impact Fragmentation, Meteorites, Ordinary Chondrites, Kinetic Impact Deflection

1. Introduction

Kinetic impact deflection, which was demonstrated by the NASA Double Asteroid Redirection Test (DART) spacecraft [1], is regarded as the most mature technology currently available for deflection of a monolithic asteroid up to a few hundred meters in diameter that is on a collision course with the Earth [2]. However, a successful kinetic impact deflection requires a knowledge of the momentum added by the impact or sequence of impacts as well as the maximum kinetic energy that can be deposited in the target without fragmentation, since this could leave a fragment of the target on a collision course with the Earth.

The momentum transferred to a monolithic rock target in a hypervelocity kinetic impact is observed to be greater than the original momentum of the projectile because of the ejection of cratering debris in a direction approximately opposite to the flight direction of the projectile. In a cratering impact on a monolithic target the recoil momentum has contributions from two factors:

1) the momentum of the impactor, and,
2) the momentum provided by the crater ejecta.

The total momentum transferred in a cratering impact is characterized by a factor β, which is the ratio of the increase in momentum of the target to the momentum of the projectile, where:

$$\beta = 1 + p_e/p_i \qquad \text{(Equation 1)}$$

where p_e is the momentum of the crater ejecta and p_i is the impactor momentum. So, β is 1 in the absence of crater ejecta and (β -1) is the momentum enhancement from the crater ejecta.

To avoid fragmentation, which could leave a large piece of the target asteroid on a collision course with Earth, the maximum change in velocity, ΔV_{max}, that can be achieved in a single kinetic impact is restricted by the requirement:

$$\Delta V_{max} = 2\ \beta\ Q^*_F/v_i \qquad \text{(Equation 2)}$$

where Q^*_F is the energy per unit target mass where the outcome of an impact transitions from cratering to fragmentation, and v_i is the speed of the impactor relative to the asteroid [3]. Thus, both β and Q^*_F must be known for the asteroid in question in order to design a successful kinetic impact deflection mission.

Modeling of hypervelocity impacts has provided insights into the expected dependance of collisional outcomes, particularly β and Q^*_F, on the strength and porosity of the target asteroid. Compaction of porous material is expected to help absorb the impact energy and reduce the transmission of shock, localizing much of the damage to the immediate region of the impact [4]. The impact modeling generally indicates that lower strength and/or higher porosity increases the collisional survival of a monolithic asteroid by requiring a higher energy for fragmentation [5, 6]. However, most of this modeling employs the physical properties of terrestrial rocks.

Asteroids span a wide diversity of mineralogical compositions, porosities, and strengths. Stickle et al. [5, 6] showed that the two most important physical properties

of the target affecting the modeled outcome of hypervelocity impact are the target strength and the target porosity. Thus, a knowledge of the strength, porosity, and likely the mineralogical composition of the target asteroid are each critical in insuring a successful kinetic impact deflection. The mineralogical composition of an asteroid can be determined remotely by reflection spectroscopy using terrestrial or space-based telescopes. However, the porosity of an asteroid is usually determined by gravitational perturbation. This requires either another relatively nearby, large asteroid or a flyby spacecraft. A strength determination generally requires a lander spacecraft to sample and test the underlying bedrock.

Meteorites provide laboratory samples of their asteroidal parent bodies, allowing measurement of the porosity and strength of samples of a variety of asteroid parent bodies. The recovered meteorites provide direct evidence for the diversity of mineralogies, strengths, and porosities among the Near-Earth Objects (NEOs). However, the weakest meteors fragment so severely during atmospheric deceleration that this group is not well sampled by the meteorites since only dust survives.

The recovered meteorites range from the weak, highly porous CI1 carbonaceous chondrites like Orgueil to the strong, low porosity iron meteorites like Canyon Diablo. The types and relative frequencies of meteorite falls provide some indication of the mineralogy, porosity, and strength range of the population of NEOs. The recovery of observed meteorite falls provides an indication of the relative abundance of each type in near-Earth space. Iron meteorites constitute less than 4% of all falls, stony-iron meteorites about 1.0%, and stony meteorites about 95%.

The ordinary chondrites are the most common stony meteorites that fall to Earth. Among the ordinary chondrites, there are three distinct types based on their mineralogies: the high-iron or H-type, the low-iron or L-type, and the very low iron or LL-type. The physical properties, including the mineralogies, the porosities, and the compressional and tensile strengths, of the stone meteorites, which constitute about 95% of all meteorite falls, were summarized in reviews by Flynn et al. [7] and Ostrowski and Bryson [8]. These reviews are consistent with the observation of Slyuta et al. [9] that: “There are no analogues among terrestrial igneous and sedimentary rocks and ores… [for the] set of physical and mechanical properties of the meteorites.” Slyuta et al. [9] indicated that knowledge of meteorite or meteorite-analog physical properties is critical to estimating the hazard of asteroidal impacts, creating engineering models for asteroid sample collection, and understanding the requirements for asteroid deflection.

2. Samples

To characterize the response of asteroid material to hypervelocity impacts we performed hypervelocity impact cratering and disruption experiments on three L-type ordinary chondrite meteorites, Aba Panu, Northwest Africa 869 (NWA 869), and Saratov. Since all three a L-type ordinary chondrites, they have very similar mineralogies, and thus similar remote sensing spectra. These three L-type meteorites were selected for our study because they were minimally weathered by exposure on the Earth, they were not severely shocked during residence near the surface and during ejection from their parent bodies, and they were available in sufficient quantity and size for the experiments. These three L-type ordinary chondrites span most of the strength range and much of the porosity range of the ordinary chondrite meteorites.

Table 1: Physical Properties and Impact Outcomes for three L-type Meteorites.

Meteorite	Type	Porosity (%)	Comp. Strength (MPa)	Speed of Sound (m/s)	β	Q^*_C J/kg)	Q^*_F (J/kg)	ΔV_{max} at ~5 km/s
Aba Panu	L3	3.1	438	5,100	3.7	1,230	680	1.01
NWA 869	L3-6	7.8	87	3,280	2.5	1,990	1320	1.32
Saratov	L4	14.1	0.97	2,350	2.3	1,090	660	0.61

We performed physical properties measurements, including the bulk and grain densities, allowing determination of the porosity, the unconfined compressive strength, the speed of sound, and Young's modulus on each of the three meteorites (Table 1). The grain volume was determined using Ideal Gas Pycnometry and the bulk volume was determined by laser scanning to target, as described by Macke et al. [10, 11]. These values were used to determine the grain density (ρ_g) and the bulk density (ρ_b) of each target type. The target porosity (P) was then determined using:

$$P = 1 - \rho_b/\rho_g \qquad \text{(Equation 3)}$$

The unconfined compressive strengths of NWA 869 and of Saratov were measured on 1 cm cubes of each meteorite by applying a pressure across two opposite faces of each cube using a hydraulic press to slowly increase the pressure until failure occurred. The strength of Aba Panu is from Cotto-Figueroa et al. [12] The speed of sound of Aba Panu and NWA 869 were measured using an ultrasonic thickness gauge in a mode that determines the sound speed when the sample thickness is known [13]. The speed of sound of Saratov samples was determined in earlier work [14].

These three L-type ordinary chondrites selected for our measurements span most of the range of porosity, and strength of the ordinary chondrite meteorites.

Aba Panu is a low porosity L3 ordinary chondrite. It is a fresh fall, having a low degree of terrestrial weathering (W0), but is somewhat shocked (S4).

NWA 869 is an intermediate porosity, brecciated L3-6 ordinary chondrite. NWA 869 is a find, but it experienced a low degree of terrestrial weathering (W1) and lesser shock (S3) than Aba Panu.

Saratov is a high porosity L4 ordinary chondrite. It is an observed fall having a low degree of terrestrial weathering (W0), but is somewhat shocked (S4).

2. Hypervelocity Impact Experiments

We conducted hypervelocity impact cratering and disruption measurements at the NASA Ames Vertical Gun Range (AVGR). Each target was suspended from the ceiling of the sample chamber on an ~2 m long fishing line. This allowed the targets to recoil freely in cratering experiments and did not interfere with the disruption in fragmentation experiments. The sample chamber was pumped to ~0.5 torr to minimize atmospheric interference with the projectile. The impactors were solid aluminum spheres having diameters of 1/16", 1/8", or 1/4" aimed at the center of each target. The speed of each impactor was determined using a laser-interrupt system. The impactor speeds ranged from 4.0 to 5.8 km/s. The AVGR and its gun chamber are described in detail by Karz et al. [15]. Some of the hypervelocity cratering and disruption results for the NWA 869

meteorite were described in an earlier paper [16], which includes a complete description of the experimental setup employed for these measurements.

For the fragmentation impacts all of the target material was recovered from the gun chamber after each impact. The mass of the largest fragment produced in the impact, M_L, was compared to the initial mass of the target, M_T. Since no two individual rocks, even from the same material, are identical in flaw distribution, shape, etc., the energy required for fragmentation is usually determined from the outcomes of a series of impacts conducted at different impactor specific energies, Q*, the impactor kinetic energy per unit target mass [17]. The energy for the onset of catastrophic disruption Q^*_C, is determined from a plot of M_L/M_T vs. Q* [17]. Q^*_C is generally regarded as the impactor energy where the mass of the largest fragment produced in the impact is one-half the target mass. Q^*_C is the value of Q* where a horizontal line at $M_L/M_T = 0.5$ intersects the best fit line to the fragmentation data (Figure 1). To determine Q^*_F, the energy for the onset of fragmentation, we extended the best fit line for M_L/M_T vs Q* to the point where it intersected $M_L/M_T = 0.98$, which corresponds to a cratering impact.

Figure 1: M_L/M_T vs Q* for Aba Panu.

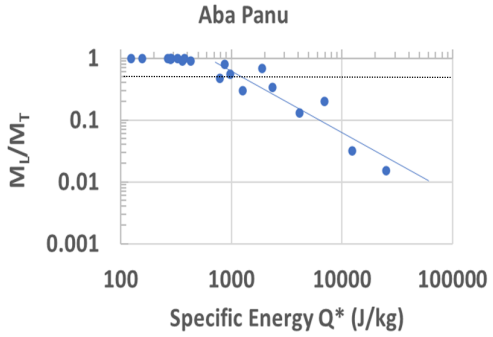

Figure 2: M_L/M_T vs Q* for NWA 869.

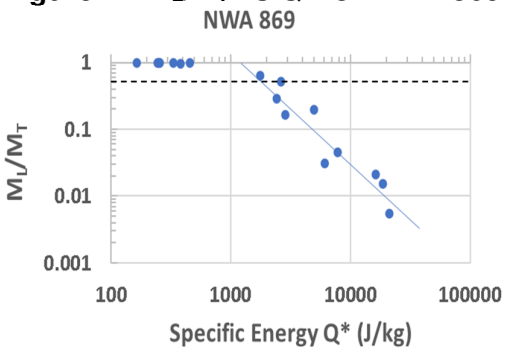

Figure 3: M_L/M_T vs Q* for Saratov.

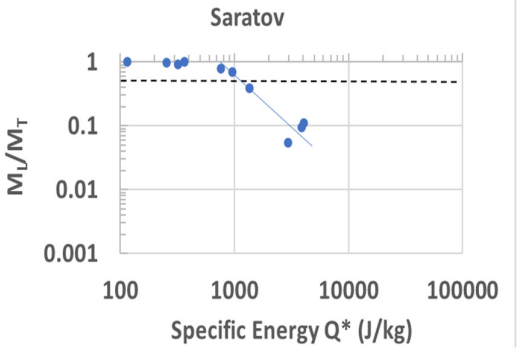

We performed ten fragmentation impacts on Aba Panu at specific energies ranging from 791 J/kg to 24,901 J/kg. These impacts gave M_L/M_T values ranging from 0.015 to 0.806 (Figure 1). The best fit line to this data set gives Q^*_C =1,230 J/kg and Q^*_F = 680 J/kg. The ten fragmentation impacts on NWA 869 were conducted at energies ranging from 1,764 J/kg to 21,225 J/kg resulting in M_L/M_T values ranging from 0.016 to 0.639 (Figure 2). The best fit line to these impacts gives Q^*_C =1,990 J/kg and Q^*_F = 1,320 J/kg. Seven fragmentation impacts were performed on Saratov at specific energies ranging from 708 J/kg to 4,069 J/kg resulting in M_L/M_T values ranging from 0.055 to 0.889 (Figure 3). The best fit line to these impacts gives Q^*_C =1,090 J/kg and Q^*_F = 660 J/kg.

For each cratering experiment marked grids were placed below and behind each target. A high-speed video camera was placed above the target and second high-speed video camera was placed in front of the target to record each impact. The resulting target recoil speed was determined from the target motion relative to the grids in a sequence of frames taken after each impact. From this recoil speed, the target

mass, and the impactor mass and speed we determined the value of β. We also determined the mass of the crater ejecta (M_T - M_L), measured the depth and the diameter of the crater, and determined the shape of the crater. The speeds of some of the larger ejecta fragments were also determined to ensure consistency between the measured recoil speed and the momentum carried by the crater ejecta. On the plots of M_L/M_T vs Q* these cratering impacts scatter around a horizontal line near M_L/M_T = 0.98 (Figures 1, 2, and 3)).

We performed ten cratering experiments on Aba Panu at specific energies ranging from 124 J/kg to 430 J/kg (Figure 1). These impacts gave a value of β = 3.7. The mass of the crater ejecta ranged from 1 g to 5 g. with a mean of 2.8 g. We performed seven cratering experiments on NWA 869 at specific energies ranging from 165 J/kg to 460 J/kg (Figure 2). These impacts gave a value of β = 2.5. The mass of the crater ejecta ranged from <0.5 g to 5 g. with a mean of 2.6 g. We performed four cratering experiments on NWA 869 at specific energies ranging from 115 J/kg to 363 J/kg (Figure 3). These impacts gave a value of β = 2.3. The mass of the crater ejecta ranged from 2 g to 3 g. with a mean of 2.3 g. The craters in Aba Panu and NWA 869 were approximately bowl shaped with depths approximately one-half their diameters. The craters in Saratov were more elongated, approximating a cylindrical shape.

3. Discussion

Saratov has the lowest compressive strength and the highest porosity of any of these three, L-type ordinary chondrites we measured. Based on hydrocode modeling, Saratov was expected to be the most resistant of the three L-type ordinary chondrites to fragmentation or disruption (i.e., have highest Q^*_F and Q^*_C). However, Saratov had the lowest Q^*_F and Q^*_C of these three meteorites.

The ordinary chondrite meteorites have a two-component structure: strong, low porosity chondrules consisting of crystalline olivine or pyroxene, embedded in a weaker, more porous matrix. The increase in porosity generally corresponds to an increase in the matrix porosity, leaving larger pore spaces that result in a decrease in the connectivity between the chondrules. This is demonstrated by the systematic decrease in the speed-of-sound from Aba Panu to NWA 869 to Saratov (Table 1).

Lewis et al. [18] used X-ray microtomography (µCT) and scanning electron microscopy to examine the abundance and distribution of porosity in Saratov. They found the porosity of the chondrules to be 1% to 2% by volume, and inferred a porosity of the matrix to be 40 to 60%. The highly porous matrix in Saratov provides only minimal, weak contacts between the chondrules. This is consistent with the low unconfined compressive strength, only 0.97 MPa, and low speed of sound, only 2,350 m/s, measured in Saratov samples.

The ordinary chondrite structure consisting of strong chondrules weakly held together by a minimal amount of matrix appears to be structurally similar to sintered spheres. Love et al [19] performed hypervelocity impact disruptions on four sintered glass sphere targets. None of their targets matched the strength and porosity of Saratov, so they do not provide a direct comparison to Saratov. Their lowest unconfined compressive strength target was 2 MPa, roughly comparable to Saratov, but that sample had a porosity of 60%. They impacted two targets with roughly the same porosity (37% and 39%) which differed in unconfined compressive strength by more than a factor of five (7.9 and 44 MPa), and found their Q^*_C values differed by a factor of two. To explain this difference, they used a result from Horz et al. [20], who

Fig. 4: Plot of log $Q^*_C/S^{0.45}$ vs. log (1 – P).

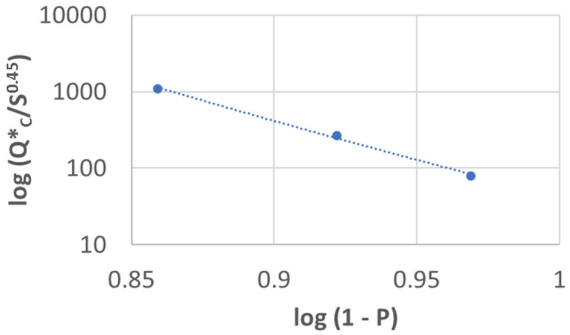

Fig. 5: Plot of log $\beta/S^{0.45}$ vs. log (1 – P).

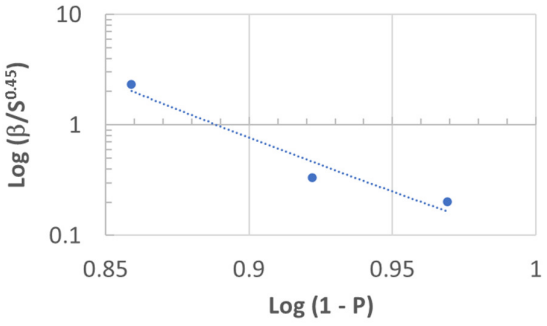

indicated that Q^*_C was proportional to $S^{0.45}$. They found a power law dependence between $Q^*_C/S^{0.45}$ and (1 – P).

Following their approach, we divided the Q^*_C values we determined for each of the three L-chondrites by $S^{0.45}$, and plotted log ($Q^*_C/S^{0.45}$) versus log (1 – P). We followed Love et al. [19] in plotting against (1 – P) since a power law cannot accommodate P = 0. The resulting log-log plot (Figure 4) shows a clear linear trend, with an R^2 value of the fit equal to 0.99. This indicates that, at least for these three L-type ordinary chondrites, which span most of the range of strength and porosity of the L-type ordinary chondrites, the effects of unconfined compressive strength and porosity can be separated. The resulting dependence of Q^*_C on S and P is:

$$Q^*_C = 42.25\ S^{0.45}\ (1 - P)^{-21.7} \qquad \text{(Equation 4)}$$

where Q^*_C is in J/kg for S in MPa.

The β values for these three L-type ordinary chondrites follow the pattern expected from hydrocode modeling, with a progressive decrease in β with increasing porosity. However, β is greater than 2 for each of the three L-type ordinary, indicating that the crater ejecta contributes more momentum to the recoil than the direct transfer of momentum by the impactor, even for the target with the highest porosity. The amount of momentum transferred by the crater ejecta (β - 1) for the two porous meteorite targets, NWA 869 and Saratov, significantly exceeds the modeled values for targets of these porosities and impact speeds [21, 22], although modeling by Bruk Syal et al. [21] gives higher β values for extremely weak targets (cohesive strength = 100 kPa) . Some hydrocode models give (β– 1) <0.4 for targets with porosity like Saratov [22]. These β values exceeding 2 for the porous meteorites are consistent with an earlier measurement of β = 2.1 for highly porous (estimated porosity of 70 to 85% based on measurement of a bulk density of ~0.5 g/cm^3) terrestrial basalt [23].

The mass of the crater ejecta was roughly the same for each of the three types of targets. Since β decreases with increasing porosity, this indicates the mean ejecta velocity decreased with increasing target porosity.

We tested if the same dependence on $S^{0.45}$ might explain the decrease in β with porosity. The plot of log ($\beta/S^{0.45}$) versus log (1 – P) is consistent with a straight line (Figure 5), suggesting that, for these three L-type ordinary chondrite targets, the effects of unconfined compressive strength and porosity on β are also separable. The resulting equation is:

$$\beta = 0.086\ S^{0.45}\ (1 - P)^{-20.8} \qquad \text{(Equation 5)}$$

where S is in MPa. As with the Q^*_C dependance, β shows a very strong dependance on porosity (1 – P), with almost the same exponent as we found for the Q^*_C dependence on (1 – P). This is consistent with results by Holsapple and Housen [24], who also found that β depended strongly on porosity.

The determination of Q^*_F and β allows us to use Equation 1 to determine the maximum change in velocity (ΔV_{max}) that could be imparted by a single kinetic impact without disrupting the target at the 5 km/s impactor speed employed in our experiments. For the low porosity meteorite Aba Panu ΔV_{max} = 1.01 m/s, for the intermediate porosity meteorite NWA 869 ΔV_{max} = 1.32 m/s, and for the high porosity meteorite Saratov ΔV_{max} = 0.61 m/s.

4. Conclusions

Based on hydrocode modeling, Saratov, which has the lowest compressive strength and the highest porosity of the three L-type ordinary chondrites we studied, would be expected to require the highest specific energy, Q^*_C, for the onset of catastrophic disruption. Contrary to this expectation, Saratov has the lowest Q^*_C of these three L-type ordinary chondrite meteorites. The intermediate porosity and intermediate strength meteorite, NWA 869, has the highest Q^*_C of the three meteorites, almost a factor-of-two higher than either Aba Panu or Saratov.

Although the data set is quite limited, these three L-type ordinary chondrites span almost the entire ranges of porosity (P) and unconfined compressive strength (S) reported in the literature for ordinary chondrite meteorites [7]. For these three L-type ordinary chondrites, both Q^*_C and β depend on $S^{0.45}$, as suggested by Horz et al. [20] for lunar rocks. Each shows a very strong dependence on (1 – P), with almost the same exponent in each case, -21.7 for Q^*_C and -20.8 for β. The good correlation of the best fit line indicates that, at least for these three L-type ordinary chondrites, the effects of unconfined compressive strength and porosity can be separated, and that the behavior of Q^*_C and β are both very strongly dependent on sample porosity.

The measured values of β decrease with increasing porosity, as expected from hydrocode modeling. However, β exceeds 2.0 for all three of these L-type ordinary chondrites. This indicates that, in each case, the momentum transferred by the crater ejecta exceeds the direct momentum transfer from the impactor. For both the intermediate porosity NWA 869 and the high porosity Saratov cratering impacts, the momentum enhancement from the crater ejecta is much higher than expected for strong, medium to high porosity targets from hydrocode modeling [21, 22].

The mean crater ejecta mass is approximately the same for each of the three meteorites. Ejecta mass and ejecta speed each affect the recoil. Since the ejecta masses are approximately the same for these three target types, the measured decrease in β indicates that the ejecta speed decreases with increasing porosity. This is consistent with observations by Love at al. [19]. who found a decrease in ejecta speed with increasing target porosity.

The maximum change in velocity that could be imparted by a single kinetic impact without fragmenting the target is within a factor-of-two for these three L-type ordinary chondrites, despite that large differences in porosity and strength. This suggests that simply establishing that a monolithic asteroid is an L-type ordinary chondrite may be sufficient for the design of a deflection mission.

Acknowledgments

This work was funded by a NASA Yearly Opportunity for Research in Planetary Defense grant, #80NSSC22K0241. The NWA 869 measurements were funded by an earlier NASA Solar System Workings grant, #NNX15AM22G. We were assisted in these measurements by Sam Strait, Ian Strait, two Alma College students, Haley Willman and Alexis Rolling and two SUNY-Plattsburgh students, Taylor Pytel and Hunter Wheeler-Cooney. We thank the AVGR crew, C. Cornelison, D. Bowling, F. Perez, A. Parrish, and J. P. Wiens, whose efforts made this project possible.

References

[1] Cheng A. F., Agrusa H. F., Barbee B. W., et al., Momentum transfer from the DART mission kinetic impact on asteroid Dimorphos, Nature (2023), 616,457–460.

[2] Shapiro, I. et al., Defending Planet Earth, National Academies Press (2010) doi:https://doi.org/10.17226/12842.

[3] Flynn, G. J., D. D. Durda, M. M. Strait, R. J. Macke, Limits on Kinetic Impact Deflection of Asteroids from Laboratory Hypervelocity Cratering and Disruption of Meteorites and Analogs**,** HVIS 2022, V001T06A002, https://doi.org/10.1115/HVIS2022-16

[4] Holsapple, K., I. Giblin, K. Housen, A. Nakamura and E. Ryan (2002) Asteroid Impacts: Laboratory Experiments and Scaling Laws, In: *Asteroids III* (eds. W. F. Bottke Jr.,; A. Cellino, P. Paolicchi and R. P. Binzel), University of Arizona Press, 443-462.

[5] Stickle, A., Bruck Syal, M., Cheng, A. F., Collins, G. S., Davison, T. et al.. Benchmarking impact hydrocodes in the strength regime: Implications for modeling deflection by a kinetic impactor. Icarus (2020) 338, pp 113446. ff10.1016/j.icarus.2019.113446ff.

[6] Stickle, A. M. et al. “Effects of Impact and Target Parameters on the Results of a Kinetic Impactor: Predictions for the Double Asteroid Redirection Test (DART) Mission” *Planet. Sci. J.*, 3:248 (2022), 29 pp. https://doi.org/10.3847/PSJ/ac91cc

[7] Flynn, G. J., G. J. Consolmagno, P. Brown, R. J. Macke (2018) Physical properties of the stone meteorites: Implications for the properties of their parent bodies, Geochemistry, 78**,** 269-298.

[8] D. Ostrowski and K. Bryson (2020) Laboratory examination of the physical properties of ordinary chondrites, Meteoritics & Planetary Science 55, 2007–2020.

[9] Slyuta, E.N., S. M. Nikitin, A. V. Korochantsev, and C. A. Lorents (2008) Physical and mechanical properties of Sayh al Uhaymir 001 and Ghubara meteorites, Lunar and Planetary Science Conference XXXIX (2008) Abstract #1056.

[10] Macke R. J., Britt D. T. and Consolmagno G. J “New pycnometer design for thin-sliced meteorites” *Lunar and Planetary Science Conference XLIV* (2013) Abstract #1398).

[11] Macke R. J., Kent J. J., Kiefer W. S. and Britt D. T. “3D-Laser-Scanning Technique Applied to Bulk Density Measurements of Apollo Lunar Samples,” Lunar and *Planetary Science Conference XLVI* ((2015) Abstract #1716.

[12] Cotto-Figueroa, D. et al. “On the Strength of the Aba Panu (L3) Meteorite: Implications for Hazard Mitigation” *Lunar and Planetary Science Conference LI* (2020) Abstract #2646.

[13] Pytel, T. et a. (2023) Speed-of-sound Measurements on Meteorite samples, 54th Lunar and Planetary Science Conference, LPI Contrib. No. 2806, Abstract# 1246.
[14] Flynn, G. J. (2004) Physical properties of meteorites and interplanetary dust particles: clues to the properties of meteorite and their parent bodies" Earth Moon Planets 95, 361-374
[15] Karcz, J. et al. "The Ames Vertical Gun Range" Lunar and Planetary Science Conference XLVII (2016) Abstract #2599.
[16] Flynn, G. J. et al. (2018) Hypervelocity cratering and disruption of the Northwest Africa 869 ordinary chondrite meteorite: Implications for crater production, catastrophic disruption, momentum transfer and dust production on asteroids, *Planetary and Space Science*, 164, 91-105.
[17] Fujiwara, A. et al. (1989) Experiments and Scaling Laws for Catastrophic Collisions (1989) in *Asteroids II (eds.:* R. P. Binzel, T. Gehrels, and M. S. Matthews), University of Arizona Press, Tucson, 240-265.
[18] Lewis et al. (2018) Chondrule porosity in the L4 chondrite Saratov: Dissolution, chemical transport, and fluid flow Geochimica et Cosmochimica Acta, Volume 240, 293-313.
[19] Love, S. G., F. Horz, and D. E. Brownlee (1993) Target Porosity Effects in Impact Cratering and Collisional Disruption, Icarus, 105, 216-224. spheres.
[20] Horz, F. et al. (1975) Catastrophic Rupture of Lunar Rocks: A Monte Carlo Simulation, The Moon, 13, 235-258.
[21] Bruck Syal, M., J. M. Owen, and P. L. Miller (2016) Deflection by kinetic impact: Sensitivity to asteroid properties, *Icarus*, 269, 50-61.
[22] Jutzi, M. and P. Michel (2014) Hypervelocity impacts on asteroids and momentum transfer I. Numerical simulations using porous targets, Icarus, 229, 247-253.
[23] Flynn, G. J. et al. (2015) Hypervelocity Cratering and Disruption of Porous Pumice Targets: Implications for Crater Production, Catastrophic Disruption, and Momentum Transfer on Porous Asteroids, Planetary and Space Science, 107, 64-76.
[24] Holsapple, K. A., Housen, K. R. (2013) Mitigation by Impacts: Theory, experiments, and code calculations https://iaaspace.org/wp-content/uploads/iaa/Scientific%20Activity/conf/pdc2013/IAA-PDC13-04-04.pdf